SRTTU
Journal of Computational and Applied Research in Mechanical Engineering
jcarme.sru.ac.ir
JCARME
ISSN: 2228-7922

Large eddy simulation of non-reactive flow in burners

M. Zakyani[a,*]

[a]*Aerospace Research Institute (ARI), Tehran, 1465774111, Iran*

Article info:

Article history:

Received: 00/00/0000
Accepted: 00/00/0018
Revised: 00/00/0000
Online: 00/00/0000

Keywords:

Large Eddy Simulation,
Sub-Grid Scale Models,
Constant Smagorinsky Model,
Dynamic Smagorinsky Model,
Dynamic WALE Model.

[*]**Corresponding author:**
zakyani@ari.ac.ir

Abstract

Large Eddy Simulations of non-reactive Delft II and Sydney bluff body flow are performed using different sub-grid scale models. Simulation of non-reactive burners is useful when studying flow characteristics inside reactive burners. As turbulent combustion simulation is rather an intricate task, it is helpful to study cold air flow inside the combustion chamber before igniting the chamber. In order to study the flow inside the mentioned test cases, different sub-grid scales model i.e., Constant Smagorinsky, dynamic Smagorinsky and dynamic WALE model are used to model the unresolved small scales. For the numerical simulations, a finite volume in-house code is used. The code adopts the projection method to solve the fluid flow equations. A second order accurate scheme is used for spatial discretization. The time integration is done using second order accurate predictor-corrector scheme. For solving the resultant pressure Poisson equation, TDMA (Tridiagonal Matrix Algorithm) is used with multi-grid convergence acceleration. Generally, the results show good agreement with available experimental data. As expected, the dynamic WALE model performs better than the other models. To further improve the results, a rather realistic type of velocity inlet boundary conditions applied to Sydney bluff body flow i.e., digital filter velocity inflow boundary conditions. The results show drastic improvement using digital filter inflow that is mainly due to turbulent nature of the flow field.

1. Introduction

Jet flows have long been under investigation by scientists and engineers due to their practical importance in many industrial applications and natural phenomena, e.g. Batchelor [1]. It naturally occurs at the exit nozzle of airplanes turbofan engines, in the turbine blade cooling, and it is essential for injecting fuel into the combustion chamber of internal combustion engines. Laminar jets are well studied using analytical fluid dynamics methods, e.g. Schlichting and Gersten [2]. However, turbulent jets which occur in significant industrial applications are normally studied numerically due to their complexity. Jet in cross flow, impinging jets and jets with coaxial secondary stream are different types of jets vastly studied. A comprehensive review of the literature on jets can be found in Ball et al. [3]. Jets with coaxial secondary stream are studied here due to their paramount importance in many practical applications. These kinds of fluid flows frequently appear in studying turbulent combustion in burners where the fuel jet is carefully mixed with coaxial secondary air

stream, e.g. Branley and Jones [4]. To have a complete combustion which by itself is important for lower pollutant emission and better combustion efficiency, fuel jet and oxidizer co-flow should mix evenly in the combustion chamber. With the continuous development of digital computers and help of Computational Fluid Dynamics (CFD), many physical aspects of jet flows are better understood. State-of-the-art turbulence models perform a crucial role in our ability to predict and understand such fluid flow phenomena like jets.

Two widely used turbulence modeling approaches, i.e. Reynolds Averaged Navier-Stokes (RANS) and Large Eddy Simulation (LES), are frequently used to accurately simulate and predict turbulent flows, e.g. Wilcox [5]. In the current work, LES is properly used to study velocity field of turbulent jets with secondary axial co-flow. LES showed promising results in turbulent flow simulations especially when large-scale energy containing eddies are resolved. The most widely used LES model was proposed by Smagorinsky [6]. He naturally assumed that the eddy viscosity was proportional to the sub-grid characteristic length scale Δx and to the characteristic turbulent velocity based on the second invariant of the filtered field deformation tensor. The scholarly literatures on LES and its applications are so vast and diverse that interested readers are referred to review articles of Lesieur and Metais [7], Piomelli [8] and Zhiyin [9].

The first published study of fluid jets dates back to almost 100 years ago according to Ball et al. [3]. However, studying jets using LES is a relatively new subject with first results appeared in the 1980s. Nevertheless, a more recent work by Bogey et al. [10] adopted explicit filtering with and without dynamic Smagorinsky model to simulate a round free jet at Mach number $M = 0.9$. They accurately reported the contributions of molecular viscosity, filtering and dynamic Smagorinsky model to energy dissipation. They reasonably concluded that alternatives to the eddy-viscosity approach by explicitly applying a selective filter to the flow variables would result in minimized dissipation of energy at larger scales. Due to importance of inflow turbulent condition, Abboud and Smith [11] used a digital filter method and a synthetic eddy method in studying flow field of a coaxial turbulent jet. They showed using a synthetic turbulent inflow velocity boundary condition will drastically improve the results. Large eddy simulations of the turbulent flows of twin parallel jets are also performed by Li et al. [12] which is important in development of next generation nuclear reactors. Other notable application typically includes jet into cross flows, which typically occurs in turbine blade cooling, fuel nozzle discharge and VTOL aircrafts. Jones and Wille [13] used LES to simulate a plane jet in a cross-flow. di Mare et al. [14] and Majander and Siikonen [15] adopted the LES to simulate a round jet penetrating into a cross flow. They were able to properly capture the counter-rotating vortex pair, traveling in the stream-wise direction.

The prediction of the jet noise emanating from aircraft nozzles represents another application of jet flows. Bodony and Lele [16] and DeBonis [17] provide a comprehensive review of the relevant research in this field.

Moreover, in a combustion chamber, the fuel jet coming from a fuel nozzle penetrates into the air stream and after sufficient mixing it will combust. A review of the use of LES for simulating combustion systems can be found in Pitsch [18]. Kim et al. [19] used LES to simulate a lean premixed dry low-NOx combustion chamber. The specific purpose was to study the operational capability of LES for design of realistic hardware. di Mare et al. [14] applied standard Smagorinsky-Lilly to simulate a model gas turbine combustor. They could adequately capture the complex flow pattern inside the combustion chamber successfully. There have been many fundamental researches in using LES in combustion. Pitsch and Steiner [20] used dynamic procedure to fine-tune the Smagorinsky constant for the simulation of Sandia flame D. Branley and Jones [4] used also the dynamic Smagorinsky procedure to simulate hydrogen diffusion flames. Navarro-Martinez and Kronenburg [21] presented results for the Sydney bluff-body burner using the dynamic Smagorinsky model.

In this paper, the potential effects of various SGS models on two types of jet flows are investigated. These flows are primarily used to

study combustion of the fuel jet in surrounding stream of air. This type of flow typically happens in combustion chambers of gas turbines and jet engines when fuel jet mixes and burn with compressed air supplied by the compressor.

To better explain the phenomena in the combustion chamber, studying cold flow is necessary. This would help to analyze mixing of the jet in the stream of air. The mixing controls the combustion process in the chamber. After cold flow tests, normally hot test is performed to further study the phenomena.

First, Delft II non-reactive jet flow is used to compare the effects of SGS modeling and then Sydney non-reactive bluff-body is used for the comparison of the models. The first case is shear flows without wall and the second one is a shear flow with the presence of the wall. In the current study various SGS models are adopted to analyze the ability of the models in capturing important phenomena happening in the mixing chamber. In addition, the effect of inlet boundary condition is investigated to further improve the results.

2. Modeling

In LES a Favre filter is applied to the Navier-Stokes equations Sagaut [22], leading to

$$\frac{\partial \overline{\rho}}{\partial t} + \frac{\partial \overline{\rho}\tilde{u}_i}{\partial x_i} = 0 \quad (1)$$

$$\frac{\partial \overline{\rho}\tilde{u}_i}{\partial t} + \frac{\partial \overline{\rho}\tilde{u}_i\tilde{u}_j}{\partial x_j} = -\frac{\partial \overline{p}}{\partial x_i} + \frac{\partial}{\partial x_j}[\overline{\mu}(\frac{\partial \tilde{u}_i}{\partial x_j} + \frac{\partial \tilde{u}_j}{\partial x_i} - \frac{2}{3}\delta_{ij}\frac{\partial \tilde{u}_k}{\partial x_k}) - \tau_{ij}^{sgs}] \quad (2)$$

where the sub-grid scale (SGS) stress can be modeled as

$$\tau_{ij}^{sgs} - \frac{1}{3}\tau_{kk}^{sgs}\delta_{ij} = 2\mu_t(\tilde{S}_{ij} - \frac{1}{3}\tilde{S}_{mm}\delta_{ij}) \quad (3)$$

with the Favre filtered strain rate, $\tilde{S}_{ij}$, defined as

$$\tilde{S}_{ij} = \frac{1}{2}(\frac{\partial \tilde{u}_i}{\partial x_j} + \frac{\partial \tilde{u}_j}{\partial x_i}) \quad (4)$$

and μ_t represent the turbulent diffusion. In the current study, the potential effects of three different sub-grid scale models are investigated: the constant Smagorinsky model, the dynamic Smagorinsky model and a newly developed dynamic version of the WALE model Ghorbaniasl [23].

2.1. Constant Smagorinsky model

In the constant Smagorinsky approach the turbulent viscosity is obtained by a simple approximation

$$\mu_t = \overline{\rho}(C_S\Delta)^2|\tilde{S}_{ij}| \quad (5)$$

where

$$|\tilde{S}_{ij}| = \sqrt{2\tilde{S}_{ij}\tilde{S}_{ij}} \quad (6)$$

and C_S is the Smagorinsky constant. Δ is the filter width taken here as the cubic root of the local grid cell volume. $C_S = 0.1$ is used in the present work, following Lesieur and Metais [7].

2.2. Dynamic Smagorinsky model

The primary drawback of the constant Smagorinsky model in common is the unrealistic prediction of the turbulent viscosity in near-wall regions. In the constant Smagorinsky model, the turbulent viscosity on the wall does not decay as fast as anticipated. Therefore, the model has difficulties in handling wall-bounded flows. To overcome this practical limitation a damping function can be typically used in the near-wall region. However, the problem of properly tuning C_S remains a challenge with the limitations of using a damping function. The dynamic procedure proposed by Germano et al. [24] beneficially uses the scale similarity of the turbulent motion of the fluid to properly determine the Smagorinsky constant locally.

Since the approach has been described already extensively in the literature, the mathematical formulation of the dynamic Smagorinsky model is not given here. Interested readers are referred to the original paper Germano et al. [24] or the review study of Lesieur and Metais [7].

2.3. Dynamic wall adapted local eddy viscosity (WALE) model

The wall adapted local eddy viscosity (WALE) model is initially proposed by Nicoud and Ducros [25]. The model, similar to the constant Smagorinsky and dynamic Smagorinsky model, is an eddy viscosity type model. The WALE model is intentionally designed to return the correct wall variation of the sub-grid scale

viscosity. The model accounts for the strain and the rotation rate to properly obtain the eddy viscosity. Following this model, we have.

$$\mu_t = \overline{\rho}(C_w\Delta)^2|\tilde{S}_w| \quad (7)$$

where

$$|\tilde{S}_w| = \frac{(\tilde{S}^d_{ij}\tilde{S}^d_{ij})^{3/2}}{(\tilde{S}_{ij}\tilde{S}_{ij})^{5/2}+(\tilde{S}^d_{ij}\tilde{S}^d_{ij})^{5/4}} \quad (8)$$

and

$$\tilde{S}^d_{ij} = \frac{1}{2}(\tilde{g}^2_{ij}+\tilde{g}^2_{ji}) - \frac{1}{3}\tilde{g}^2_{kk}\delta_{ij} \quad (9)$$

where

$$\tilde{g}^2_{ij} = \frac{\partial\tilde{u}_i}{\partial x_k}\frac{\partial\tilde{u}_k}{\partial x_j} \quad (10)$$

C_w represent the model parameter and should be adjusted accordingly. Like the constant Smagorinsky model, the dynamic procedure proposed by Germano et al. [24] can be appropriately applied to the WALE model. Ghorbaniasl and Lacor [26] developed a dynamic version of the model to precisely adjust the model parameter locally in time and space. The model showed promising results when applied to the periodic channel flow.

3. Numerical algorithm

The LES code used for solving the Navier-Stokes equations is an in-house code Zakyani [27]. The flow equations are solved using the projection method of Chorin [28]. The resulting Poisson equation for the pressure is solved efficiently with a tridiagonal matrix algorithm. To accelerate convergence, the multi-grid method is used. The convective fluxes are discretized with a second-order central scheme for the momentum equation. A predictor-corrector method Pitsch and Steiner [20] is used for time integration of the unsteady Favre filtered Navier-Stokes equations. The code can adequately deal with variable density low Mach number flows. For completeness, the predictor-corrector method used in this study, which is 2nd order accurate in time, is short explained.

Predictor step

Using the second order Adams-Bashforth method with variable step size for time integration of the Navier-Stokes equations, the discretized momentum equations read

$$\frac{(\widehat{\overline{\rho}\tilde{u}_i})^* - (\overline{\rho}\tilde{u}_i)^n}{\Delta t^n} = \left(1+\frac{1}{2}\frac{\Delta t^n}{\Delta t^{n-1}}\right)Res_u^n - \left(\frac{1}{2}\frac{\Delta t^n}{\Delta t^{n-1}}\right)Res_u^{n-1} \quad (11)$$

where Res_u is defined as

$$\mathrm{Res}_u = -\frac{\partial\overline{\rho}\tilde{u}_i\tilde{u}_j}{\partial x_j} + \frac{\partial}{\partial x_j}\left((\overline{\mu}+\mu_t)\left(\frac{\partial\tilde{u}_i}{\partial x_j}+\frac{\partial\tilde{u}_j}{\partial x_i}-\frac{2}{3}\frac{\partial\tilde{u}_k}{\partial x_k}\right)\right) \quad (12)$$

The corrected velocity field is computed at the corrector step.

$$(\overline{\rho}\tilde{u}_i)^* = (\widehat{\overline{\rho}\tilde{u}_i})^* - \Delta t^n\frac{\partial\overline{p}^*}{\partial x_i} \quad (13)$$

where the pressure is properly obtained solving the Poisson equation

$$\frac{\partial(\widehat{\overline{\rho}\tilde{u}_i})^*}{\partial x_i} + \frac{\partial\overline{\rho}^*}{\partial t} = \Delta t^n\frac{\partial^2\overline{p}^*}{\partial x_i\partial x_i} \quad (14)$$

Corrector step

In the corrector step, applying the second order Adams-Moulton method to the Navier-Stokes system, one naturally obtains

$$\frac{(\widehat{\overline{\rho}\tilde{u}_i})^{n+1} - (\overline{\rho}\tilde{u}_i)^n}{\Delta t^n} = \frac{1}{2}Res_u^n + \frac{1}{2}Res_u^{n-1} \quad (15)$$

The corrected velocity field is computed at the corrector step.

$$(\overline{\rho}\tilde{u}_i)^{n+1} = (\widehat{\overline{\rho}\tilde{u}_i})^{n+1} - \Delta t^n\frac{\partial\overline{p}^{n+1}}{\partial x_i} \quad (16)$$

where the pressure is obtained solving the Poisson equation

$$\frac{\partial(\widehat{\overline{\rho}\tilde{u}_i})^{n+1}}{\partial x_i} + \frac{\partial\overline{\rho}^{n+1}}{\partial t} = \Delta t^n\frac{\partial^2\overline{p}^{n+1}}{\partial x_i\partial x_i} \quad (17)$$

4. Test case description and numerical computations

4.1. Delft II jet flow

The first test case studied in this research is the Delft II jet flow. The Delft II jet, which is primarily designed as a burner for Delft III non-premixed piloted flame, is a suitable test case for the empirical validation of turbulence models. The test case was studied experimentally by Stroomer [29] at Delft University. The Reynolds number based on jet diameter and jet bulk velocity is 9700. The jet bulk velocity is $U_j = 21.9m/s$ which emanates from a nozzle with the diameter of $D_j = 0.006m$. The annulus flow of air encloses the fuel jet, and the pilot enters the

domain with a bulk speed of 4.4 m/s. The burner is surrounded by a co-flow of air at 0.4 m/s. A schematic figure of the Delft II test case is depicted in Fig. 1.

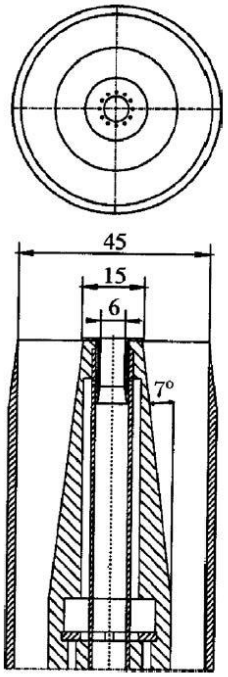

Fig. 1. Schematic picture of Delft II test case burner (jet head) taken from Merci et al. [30]

For the simulation of the Delft II test case, a cylindrical domain with $153D_j$ length and $40D_j$ diameter is used. The computational cylindrical mesh consists of $216 \times 40 \times 40$ cells with clustering in axial and radial directions near the jet region. Ultimately, the mesh is divided into 9 blocks in the axial direction for parallel computations. The mesh is presented in Fig. 2.

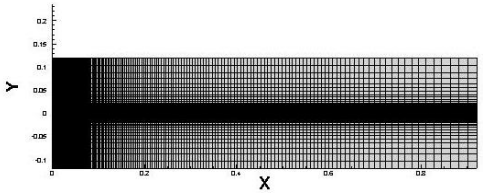

Fig. 2. Mesh generated for Delft II test case

4.2. Sydney bluff body jet flow

The second test case studied in this research is the Sydney bluff body jet flow. The Sydney bluff body jet case was also primarily designed as a burner for Sydney bluff body flame. The test case was studied experimentally by the University of Sydney. The specific details of the experiment can be found in Dally et al. [31] and Dally et al. [32]. The Sydney bluff body test case consists of a jet that emanates from a circular pipe with $D_j = 3.6mm$ diameter. A bluff body of the diameter $D_b = 50mm$, surrounds the jet. The whole bluff body is surrounded by a co-flow. The Jet velocity is $U_j = 61m/s$ and the co-flow velocity is 20 m/s. A schematic picture of the Sydney bluff body test case is displayed in Fig. 3.

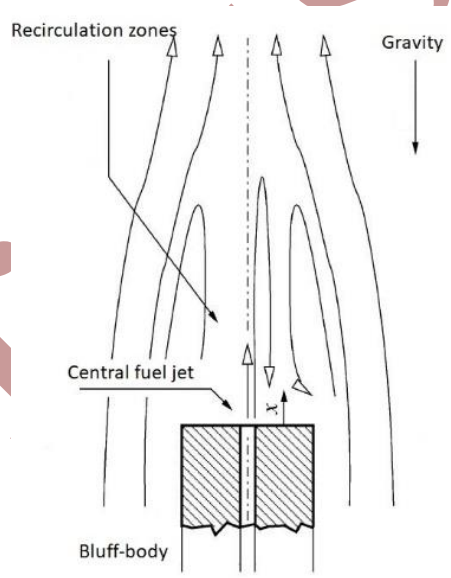

Fig. 3. Schematic picture of Sydney bluff test case taken from Kempf et al. [33]

For the simulation of the Sydney bluff body flow, a cylindrical domain with $7.2D_b$ length and $4.88D_b$ diameter is used. The cylindrical mesh consists of $192 \times 64 \times 40$ cells. For parallel computations, the mesh is carefully divided into 8 blocks in axial directions. The mesh is illustrated in Fig. 4.

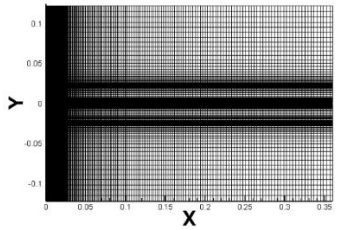

Fig. 4. Mesh generated for Sydney bluff body test case

5. Results and discussion

Results are shown for the Delft II test case in Fig. 5 & Fig. **6**. At the inlet, the velocity boundary conditions are imposed from the given experimental data, and the pressure is extrapolated. At the outlet, the pressure is set to ambient pressure, and the velocity is extrapolated. For the far-field, the velocities are set to far-field values.

To obtain the results, 10 through flow times, τ, of calculation was performed based on the jet velocity and the domain length to pass the transient time.

$$\tau \approx \frac{L_D}{U_j} \tag{18}$$

where L_D stands for the domain length and U_j represent the jet velocity. The value of the through-flow times for the Delft II case is about 0.03 seconds. An additional 10 through flow times of calculation was performed to obtain statistically averaged results.

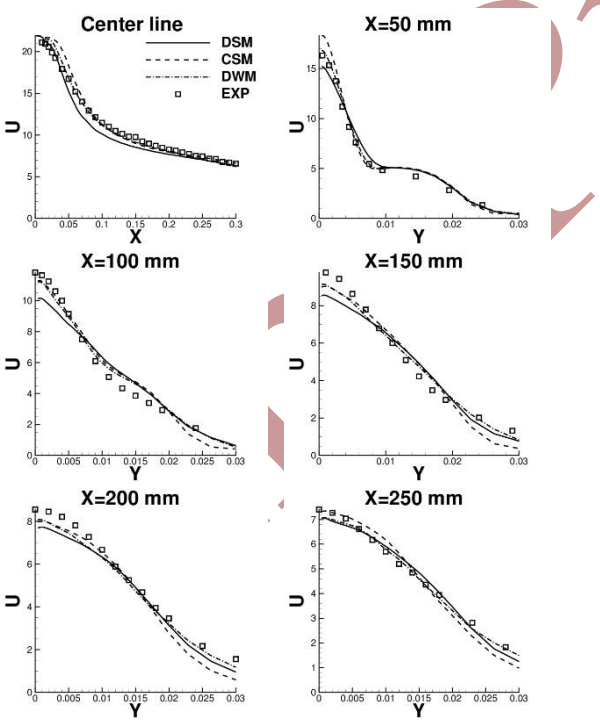

Fig. 5. Comparison of axial velocity with experimental data for Delft II test case

The comparison of the axial velocity with experimental data of Stroomer [29] is made in Fig. 5 for five different cross-sections along the centerline as well on the centerline itself. Also, Fig. 5 & Fig. **6** show the comparison between three various SGS models where CSM stands for constant Smagorinsky, DSM for dynamic Smagorinsky and DWM for dynamic WALE model.

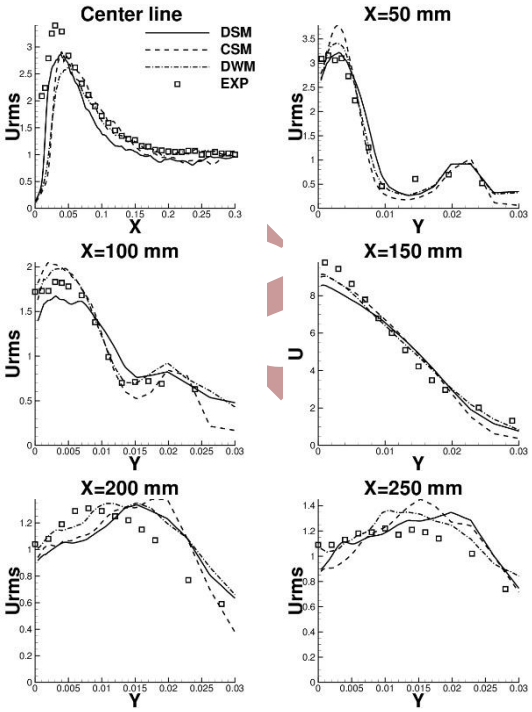

Fig. 6. Comparison of rms of axial velocity with experimental data for Delft II test case

As it is shown in the Fig. 5 & Fig. **6**, the DWM generally performs better than the DSM and the CSM model. Looking at the axial velocity in Fig. 5, it is seen that the centerline axial velocity decays faster for the DSM than the other two models. Therefore, it fails to predict the centerline velocity accurately farther downstream. In contrast, the axial centerline velocity is higher than the experimental data for the CSM especially in the near-field region of the jet. Interestingly, the DWM accurately predicts the axial centerline velocity. Reason for the superior results of the dynamic WALE is due to ability of the model to capture flows with strong shear forces. As can be seen in Eqs. (8-10), the model adjusts for high strain rate of the flow field. In the current configuration, these high strain rates happens at contact surface of the jet and coflow. Also, dynamic procedure applied to

the WALE model helps to further improve the results.

The same is true for the prediction of axial velocity in different cross-sections, especially the cross-sections close to the nozzle. As it can be seen in Fig. 5, the diffusion of the jet is very well predicted by the DWM for section $x = 50mm$ and $x = 100mm$. All three SGS models overpredict the axial velocity in the co-flow region at $7.5mm < Y < 22.5mm$. This can be explained by a lack of turbulence at the co-flow inlet profile.

For the remaining cross-sections, there are slight differences in the prediction of axial velocity. This can be explained that far from the jet, the strain rate is not too high and there is no strong shear force acting on the flow. Therefore, all models behave similarly farther downstream.

Additionally, near the edge of the domain at the far-field, the axial velocity prediction of the DWM agrees with experimental data. Despite a more accurate prediction of the axial velocity near the jet region for the CSM, as the radius increases, the axial velocity drastically deviates from the experiment. The DWM under-predicts the axial velocity near the jet region but obtains better agreement with the experiment in the co-flow region. The DWM provides a good prediction of the axial velocity for both jet and co-flow regions. Generally, in the absence of strong shear force, almost all SGS models behave similarly.

In Fig. 6, the rms of axial velocity is compared against the experimental data for three SGS models. Looking at the rms of the axial velocity along the centerline reveals that all three models underestimate the rms values. However, comparisons of the rms of axial velocity in different cross-sections reproduce the experimental results fairly well. There are no significant differences between all three SGS models in the comparison of the rms of axial velocity.

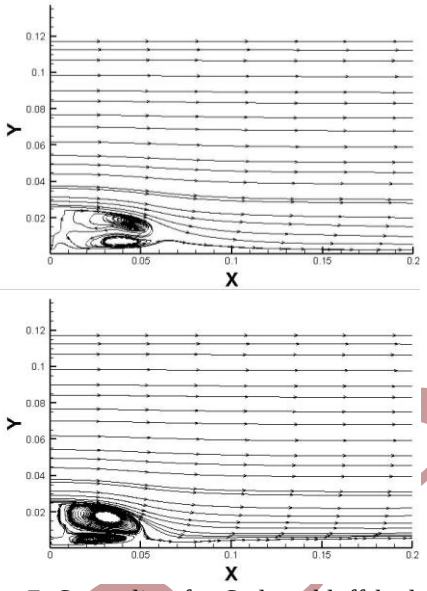

Fig. 7. Streamline for Sydney bluff body test case: without digital filter (up), with digital filter (down)

The next test case is the Sydney bluff body flow. Similar to the previous test case, to obtain the results 15 through flow times of calculation were performed to pass the transient time and then an additional 15 through flow times to obtain statistically averaged results. Similar to previous test case, the pressure is extrapolated at the inlet. At the outlet, the velocity is extrapolated and the pressure is set to ambient pressure. The treatment of the far-field boundary condition for the Sydney bluff body test case is similar to the Delft II test case. However, for imposing the inlet velocity boundary condition, two alternative methods are employed. Initially, the laminar inlet velocity boundary condition was applied and then the digital filter of Klein et al. [34] is used to further improve the results.

The Sydney bluff body test case has two distinctive shear layers. The inner shear layer forms because of the jet emanating from the center of the solid bluff body. The velocity difference between the jet and the solid bluff body produces this shear layer. The outer shear layer forms because of the flow passing over the edge of the bluff body. This develops two counter-rotating vortices behind the bluff body that can be clearly identified in Fig. 7.

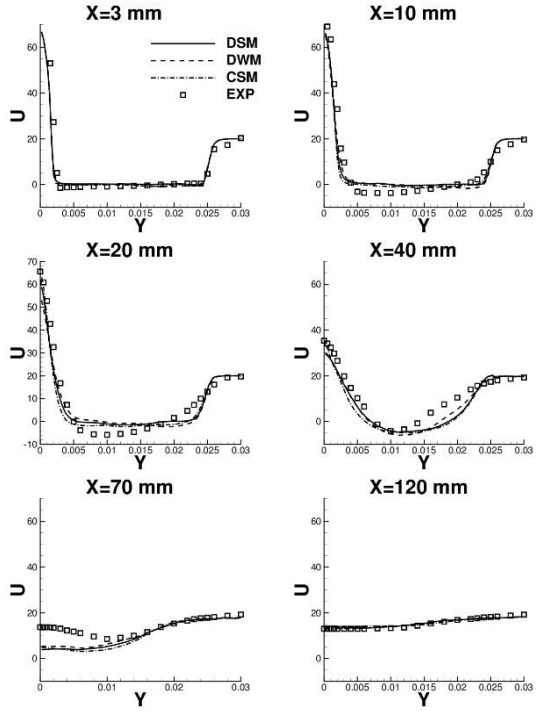

Fig. 8. Comparison of axial velocity for Sydney bluff body test case: different SGS model

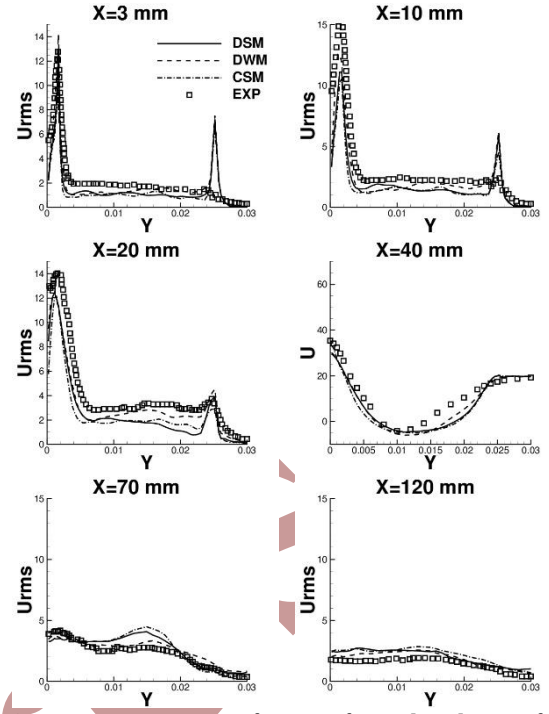

Fig. 9. Comparison of rms of axial velocity for Sydney bluff body test case: different SGS model

First, the comparison of the results for three various SGS models using laminar inlet velocity boundary condition with the experimental data of Dally et al. [31] and Dally et al. [32] is presented in Fig. 8 & Fig. **9**. The comparison of the axial velocity along six different cross-sections in the stream-wise direction is presented in Fig. 8. There are no significant differences between the results of the three SGS models. However, the DWM seems to be a bit superior to the DSM and CSM. The same conclusion as in Delft II test case is also valid here.

It is recognized in Fig. 9 that there are two peaks for the rms of the axial velocity at $x = 3mm$ and $x = 10mm$. These peaks correspond to the formation of the shear layers mentioned above.

To improve the results, a synthetic digital filter proposed by Klein et al. [34] is applied at the inlet boundary condition. For the SGS modeling, DWM is used as it has shown privileged results in comparison to other SGS models studied before. The digital filter creates a randomly generated turbulent inlet velocity boundary condition that mimic the real condition of the jet at inflow of the domain. When using a laminar inlet velocity boundary condition, the lack of turbulence at the inflow boundary condition causes over-prediction of the recirculation zone behind the bluff body. After utilizing the digital filter of Klein et al. [34], the results were improved drastically. It can be noted in Fig. 7, the point of reattachment for the digital filer is shorter than the laminar inlet. That is because increasing the momentum exchange in the shear layers will lead to stronger and more mixing.

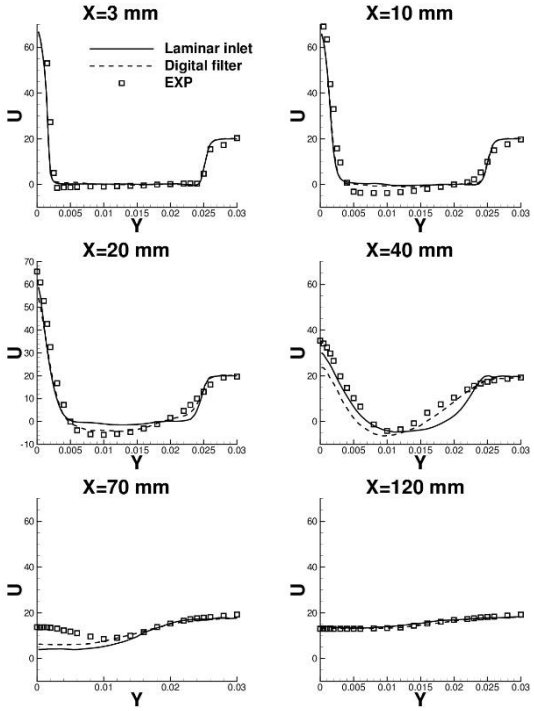

Fig. 10. Comparison of axial velocity for Sydney bluff body test case: different inlet boundary condition

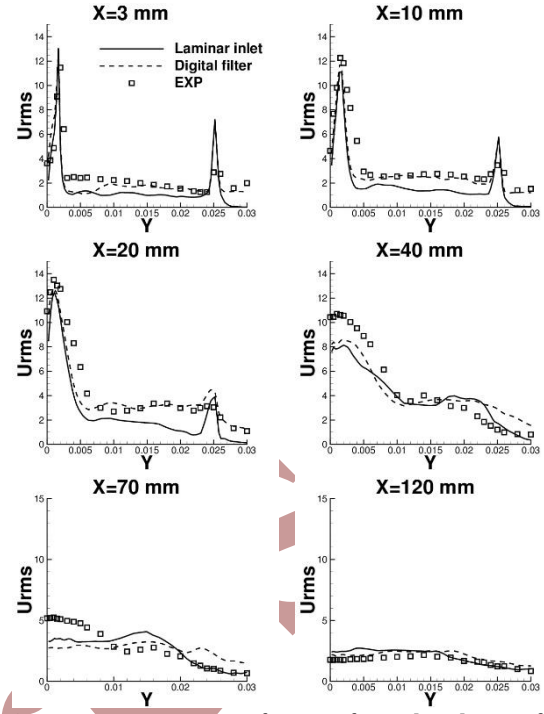

Fig. 11. Comparison of rms of axial velocity for Sydney bluff body test case: different inlet boundary condition

This is exceptionally critical for combustion applications where the fuel and the co-flow of oxidizer should mix properly to have complete combustion. The comparison between two different inlet velocity boundary conditions using the DSM for the axial and the radial velocities and their rms is shown in Fig. 10 and Fig. 11. As it can be observed in Fig. 10, at $x = 20mm$ and $x = 40mm$, where the recirculation region is located, the results are improved considerably. Additionally, it is apparent from Fig. 11 that the rms of axial velocity is improved drastically at mentioned locations due to the improved application of boundary condition.

6. Conclusion

Large eddy simulation of Delft II jet flow and Sydney bluff body jet flow performed using three different eddy-viscosity based SGS models. The constant Smagorinsky model, the dynamic Smagorinsky model, and the dynamic WALE model are used to evaluate the effects of the SGS model on the prediction of two complex jets.

First, the Delft II jet flow are studied using the three different SGS models. The results show that the dynamic WALE model is superior in prediction of Delft II test case especially near the jet region.

Next, the Sydney bluff body jet flow is investigated. It is found that the dynamic WALE model is advantageous in case of Sydney bluff body flow. This is because the model accounts for the right asymptotic behavior near solid walls and shear flows which present in the current flows.

To improve the results, the synthetic digital filter is properly used at the inlet boundary condition. It is discovered that the turbulence inlet

boundary condition causes the results improve drastically in recirculation regions. To summarize, it is found that the dynamic WALE model produces a more precise prediction of the flow field especially near the jet region when applying turbulence boundary condition for the inlet velocity.
To improve the results, it is suggested to study the flow fields using advanced technique like Detached Eddy Simulations (DES). This approach solve RANS equations in near wall regions and LES far from the wall when the flow is homogenous.

Acknowledgment

This research was funded by the Aerospace Research Institute (ARI) of the ministry of science, research and technology of the I.R. IRAN. This funding is thankfully acknowledged.

References

[1] G. K. Batchelor, *An Introduction to Fluid Dynamics*, 1st ed., Cambridge University Press, Cambridge, (2000).
[2] H. Schlichting and K. Gersten, *Boundary-Layer Theory*, 9th ed., Springer, Berlin, (2017).
[3] C. G. Ball, H. Fellouah and A. Pollard, "The flow field in turbulent round free jets", *Prog. Aerosp. Sci.*, Vol. 50, No. 1, pp. 1-26, (2012).
[4] N. Branley and W. P. Jones, "Large eddy simulation of a turbulent non-premixed flame", *Combust. Flame*, Vol. 127, No. 1-2, pp. 1914-1934, (2001).
[5] D. C. Wilcox, *Turbulence Modeling for CFD*, 3rd ed., DCW Industries, La Canada, (2006).
[6] J. Smagorinsky, "General circulation experiments with the primitive equation", *Mon. Weather Rev.*, Vol. 91, No. 3, pp. 99-165, (1963).
https://journals.ametsoc.org/view/journals/mwre/91/3/1520-0493_1963_091_0099_gcewtp_2_3_co_2.xml
[7] M. Lesieur and O. Metais, "New trends in large-edyy simulations of turbulence", *Annu. Rev. Fluid Mech.*, Vol. 28, No. 1, pp. 45-82, (1996).
[8] U. Piomelli, "Large-eddy simulation: achievements and challenges", *Prog. Aerosp. Sci.*, Vol. 35, No. 4, pp. 335-362, (1999).
[9] Y. Zhiyin, "Large-eddy simulation: Past, present and the future", *Chinese J. Aeronaut.*, Vol. 28, No. 1, pp. 11-24, (2015).
[10] C. Bogey, O. Marsden and C. Bailly, "Investigation of the effects of initial turbulence level on the flow field properties of a subsonic jet", *Proc. of 7th International Symposium on Turbulence and Shear Flow Phenomena* Ottawa, Canada, pp. 1-6, (2011).
[11] A. W. Abboud and S. T. Smith, "Large eddy simulation of a coaxial jet with a synthetic turbulent inlet", *Int. J. Heat Fluid Flow*, Vol. 50, No. 1, pp. 240-253, (2014).
[12] H. Li, N. K. Anand, Y. A. Hassan, et al., "Large eddy simulations of the turbulent flows of twin parallel jets", *Int. J. Heat Mass Trans.*, Vol. 129, No. 1, pp. 1263-1273, (2019).
[13] W. P. Jones and M. Wille, "Large-eddy simulation of a plane jet in a cross-flow", *Int. J. Heat Fluid Flow*, Vol. 17, No. 3, pp. 296-306, (1996).
[14] F. di Mare, W. P. Jones and K. R. Menzies, "Large eddy simulation of a model gas turbine combustor", *Combust. Flame*, Vol. 137, No. 3, pp. 278-294, (2004).
[15] P. Majander and T. Siikonen, "Large-eddy simulation of a round jet in a cross-flow", *Int. J. Heat Fluid Flow*, Vol. 27, No. 3, pp. 402-415, (2006).
[16] D. J. Bodony and S. K. Lele, "Current Status of Jet Noise Predictions Using Large-Eddy Simulation", *AIAA J.*, Vol. 46, No. 2, pp. 364-380, (2008).
[17] J. R. DeBonis, "Progress towards large-eddy simulations for prediction of realistic nozzle systems", *J. Propuls. Power*, Vol. 23, No. 5, pp. 971-980, (2007).

[18] H. Pitsch, "Large-eddy simulation of turbulent combustion", *Annu. Rev. Fluid Mech.*, Vol. 38, No. 1, pp. 453-482, (2006).

[19] W. W. Kim, S. Menon and H. C. Mongia, "Large-eddy simulation of a gas turbine combustor flow", *Combust. Sci. Technol.*, Vol. 143, No. 1-6, pp. 25-62, (1999).

[20] H. Pitsch and H. Steiner, "Large-eddy simulation of a turbulent piloted methane/air diffusion flame (Sandia flame D)", *Phys. Fluids*, Vol. 12, No. 10, pp. 2541-2554, (2000).

[21] S. Navarro-Martinez and A. Kronenburg, "LES-CMC simulations of a turbulent bluff-body flame", *Proc. Combust. Inst.*, Vol. 31, No. 2, pp. 1721-1728, (2007).

[22] P. Sagaut, *Large Eddy Simulation for Incompressible Flows An Introduction*, Third ed., Springer, (2006).

[23] G. Ghorbaniasl, *Computational aeroacoustic-noise prediction using hybrid methodologies*, Ph.D. thesis, Vrije Universiteit Brussel, Brussels, Belgium, (2009).

[24] M. Germano, U. Piomelli, P. Moin, et al., "A dynamic subgrid-scale eddy viscosity model", *Phys. Fluids A*, Vol. 3, No. 7, pp. 1760-1765, (1991).

[25] F. Nicoud and F. Ducros, "Subgrid-scale stress modeling based on the square of the velocity gradient tensor", *Flow Turbul. Combust.*, Vol. 62, No. 3, pp. 183-200, (1999).

[26] G. Ghorbaniasl and C. Lacor, "Sensitivity of SGS models and of quality of LES to grid irregularity", *Quality and Reliability of Large-Eddy Simulations*, Eds. J. Meyers *et al.* Dordrecht, Springer, pp. 155-166, (2008).

[27] M. Zakyani, *Simulation of turbulent diffusion flames using large eddy simulation and conditional moment closure*, Ph.D. thesis, Vrije Universiteit Brussel, Brussels, Belgium, (2011).

[28] A. J. Chorin, "Numerical solution of the Navier-Stokes equations", *Math. Comput.*, Vol. 22, No. 104, pp. 745-762, (1968).

[29] P. P. J. Stroomer, *Turbulence and OH structures in flames*, Ph.D. thesis, Delft University of Technology, Delft, Netherland, (1995).

[30] B. Merci, D. Roekaerts and B. Naud, "Study of the performance of three micromixing models in transported scalar PDF simulations of a piloted jet diffusion flame ("Delft flame III")", *Combust. Flame*, Vol. 144, No. 3, pp. 476-493, (2006).

[31] B. B. Dally, D. Fletcher and A. R. Masri, "Flow and mixing fields of turbulent bluff-body jets and flames", *Combustion Theory and Modeling*, Vol. 2, No. 2, pp. 193-219, (1998).

[32] B. B. Dally, A. R. Masri, R. S. Barlow, et al., "Instantaneous and mean compositional structure of bluff-body stabilized nonpremixed flames", *Combust. Flame*, Vol. 114, No. 1-2, pp. 119-148, (1998).

[33] A. Kempf, R. P. Lindstedt and J. Janicka, "Large-eddy simulation of a bluff-body stabilized nonpremixed flame", *Combust. Flame*, Vol. 144, No. 1-2, pp. 170-189, (2006).

[34] M. Klein, A. Sadiki and J. Janicka, "A digital filter based generation of inflow data for spatially developing direct numerical or large eddy simulations", *J. Comput. Phys.*, Vol. 186, No. 2, pp. 652-665, (2003).